AVANCES
EN CIENCIAS E INGENIERÍAS
ARTÍCULO/ARTICLE SECCIÓN/SECTION C

Storm-Source-Locating Algorithm Based on the Dispersive Nature of Ocean Swells.

Jesús Portilla[1*]

[1] *Colegio de Ciencias e Ingenierías –El Politécnico– Universidad San Francisco de Quito*
Diego de Robles s/n y Vía Interoceánica, Quito, Ecuador
E-mail: jportilla@ymail.com

Editado por/Edited by: C. Zambrano, Ph.D.
Recibido/Received: 05/10/2012. Aceptado/Accepted: 06/10/2012.
Publicado en línea/Published on Web: 06/30/2012. Impreso/Printed: 06/30/2012.

Abstract

The dispersion relationship of ocean waves in deep water dictates that the wave velocity depends on frequency. Waves of smaller frequencies travel faster than waves of larger frequencies. Therefore, at any remote location, for a specific storm event, the wave frequency and the time of arrival are related in a linear fashion. In the present work, this property is exploited in order to derive information about the distance of the originating storms and also about the time in which those storms take place. For this analysis, wave spectral data from the ECMWF (European Centre for Medium-Range Weather Forecasts) are used. The output is verified against parameters from the meteorological model, namely atmospheric surface pressure and wind velocity. The results show that the algorithm provides space and time information in consistency with the meteorological data.

Keywords. swell, swell tracking, wind waves, ECMWF, WAM, spectral partitioning

Resumen

La relación de dispersión para olas de viento en aguas profundas indica que su velocidad depende de la frecuencia. Las olas de menor frecuencia viajan más rápido que las de mayor frecuencia. Por esta razón, en un lugar remoto y para un evento de tormenta específico, la frecuencia de las olas y su tiempo de llegada están relacionados linealmente. En el presente estudio, esta propiedad es utilizada para obtener información acerca de la distancia de la tormenta generatriz y además acerca del tiempo en el cual dicha tormenta tuvo lugar. Para este análisis se usan datos del Centro Europeo para la predicción del clima a mediano plazo (ECMWF, por sus siglas en inglés). Los resultados son verificados con parámetros del modelo meteorológico, como presión atmosférica superficial y velocidad del viento. Los resultados muestran que el algoritmo produce información de espacio y tiempo en consistencia con los datos meteorológicos.

Palabras Clave. oleaje libre, rastreo de oleaje libre, olas de viento, ECMWF, WAM, partición espectral.

Introduction

Waves generated by wind are distributed over a range of frequencies and directions. This distribution defines largely their evolution and characteristics and it is represented by the wave energy density spectrum. In conventional state-of-the-art wave modelling and analysis, wind waves are described as the superposition of a finite number of monochromatic waves (i.e., linear theory). From the solution of the linearized mass balance equation, an expression is readily obtained to relate some properties of the waves like frequency and wave number. This expression is referred to as the wave dispersion relationship because in deep-water conditions it dictates that the wave velocity is dependent on the wave frequency (see Eq. 8). This means that the longer, low-frequency waves travel faster than the shorter, high frequency waves [1]. Therefore, from the generation location itself, waves disperse from each other as they travel over the ocean surface. Shorter waves are subject to large energy dissipation rates mainly due to breaking. Contrarily, longer waves would typically leave the generation zone and propagate freely from wind influence in the form of swells. Although swells might dissipate energy for instance due to viscous effects or by interacting with the atmosphere, currents or turbulence [2, 3, 4], their energy dissipation is in general small and therefore they can travel very long distances almost undisturbed. When swell waves arrive at a particular remote location far from their generation zone, they show a typical pat-

ISSN 1390-5384

tern inherent to this dispersive nature, longer waves with lower frequencies are observed to arrive first, followed by shorter waves with higher frequencies (see fig. 2b).

Munk et al., (1963) [5] and Snodgrass et al. (1966) [6] used this property to track swell systems that travelled more than 10,000 km along a great circle from New Zeeland to Alaska across the Pacific Ocean. They found a remarkably low dissipation of swell waves outside the generation zone. This indicated that resonant interactions were less important in narrow banded swell spectra and supported the validity of linear theory for the propagation of swells [7]. More recently, swell tracking algorithms have been used in other applications related to earth sciences. MacAyeal et al., 2006 [8], and Bromirski et al., 2010 [9], for instance use it to trace swells and infragravity waves respectively, originated as far as in the Alaska region. Their results suggest that iceberg calving from the Antarctic glaciers might be associated to the mechanical effects caused by ocean waves from the North Hemisphere. Collard et al. (2009) [10] used the dispersive characteristic of waves to back trace and propagate swells observed by the Synthetic Aperture Radar (SAR) mounted on board of several satellite missions. By this approach, Collard et al. (2009) [10] were able to produce more continuous swell fields than those provided by the SAR. In addition, they predicted the propagation of swells across the ocean using observed data (e.g., Fireworks products, GlobWave 2012 [11]). Delpey et al., (2010) [12], use it as a tool to characterize the time and space structures of swells in order to derive parameters for data assimilation. The main emphasis in the present application is the characterization of the wave conditions in the Equatorial Pacific Zone, and in particular, waves in Ecuadorian waters.

Different swell systems are identified using a spectral partitioning technique [13]. The analysis is therefore carried out looking at individual swell systems. This approach allows having clean signals of the relevant variables like peak wave period and direction. A pre – processing stage consists of clustering the different wave events. Initially this step was carried out using time series of significant wave height (H_{m0}), but soon it was clear that the use of that variable was not convenient because consecutive events with comparable energy are not discernible in the H_{m0} series. This step is reported here for the sake of completeness and illustration, but it is not part of the final algorithm in which the clustering is made on the time-series of peak period (T_p). The data points clustered represent swell events originated from the same storm. The peak frequency points (inverse of the peak period) are related to the time of arrival of the individual swells in a linear fashion, but they do not perfectly follow a straight line because the data contains some variability. That variability is attributed to two possible main sources. The first is the discretization of the model, both in the spectral and in the spatial space. The second is the fact that the storm source is not static but it is moving. Moreover, its spatial length scale is relatively large. However, it is found that the variability of the time-series can actually be used as an extra piece of information since this variability, apart from the leaps of the discrete model, contains valuable information about the ranges in which the storm has been generating waves. In this regard, the confidence limits of the linear regression are computed and used in order to estimate the confidence limits for the originating distance and time. It should be noted also that the peak direction time-series also present variability, which is again associated to the displacement of the storm. This information is also used for assessing the possible location of the storm, giving different possible trajectories for the waves.

The output is verified using meteorological variables from the atmospheric model from the ECMWF [14], namely atmospheric surface pressure and wind speed and direction. The results show good skills of the algorithm for locating the storm sources. Moreover, it shows the benefits of having the output in the form of ranges rather than single point locations, because the storms themselves are very dynamic and have relatively large dimensions. This means that waves might be generated from different places within the same storm. In addition, storms are typically moving, and change intensity during their lifetime. It is also found that swell waves arriving to the Equatorial Zone come from remote places that can be located as far as from the Australian region.

Data Sources

The data used in this study consists of wave model results from the ECMWF, corresponding to the ERA – Interim archive (Simmons et al., 2006). ERA – interim is a hindcast program, run with analyzed wind fields, covering the period from 1979 to present. The data has global coverage with spatial resolution of 0.5 degree in latitude and longitude. The wave model used is WAM Cycle IV [15, 16, 17]. WAM is a state-of-the-art third generation spectral wave model that solves the wave energy balance equation defined in the spectral domain. Deep-water sink/source terms account for wind input, non-linear resonant interaction, and wave breaking dissipation. Therefore, the actual variable of the model is the wave spectrum. However, it is typical to provide users with output in the form of integral parameters like significant wave height (H_{m0}), mean wave period ($T_{m-1,0}$), and mean wave direction (θ_m). WAM is used operationally in several meteorological centers around the world, and it is routinely verified and tested [18, 19].

The wave spectrum is discretized into 24 directional and 30 frequency bins. The frequency ranges from 0.0345 to 0.5476 in geometric sequence (see ECMWF 2011 for details). The spectral data correspond to the model grid point 1 °S, 93°W, located near the Galapagos Islands, where the water depth is of about 3000m. The study period corresponds to the month of January 2008.

For verification purposes, global meteorological data from the ECMWF, corresponding also to the ERA – Interim archive are used. Particularly, surface pressure and wind vectors (speed and direction). The resolution of this data is of 1.5° in latitude and longitude.

Theoretical Background

In linear theory, the dispersion relationship (Eq. 1) relates the angular frequency (ω) with the wave number (k) and the water depth (d). In deep water the term kd approaches infinity, and its hyperbolic tangent, tanh(kd) converges to 1. Hence, the angular frequency in deep water is a function of the wave number only (Eq. 2)

$$\omega^2 = gk \tanh(kd) \tag{1}$$

$$\omega^2 = gk \qquad (deep\ water) \tag{2}$$

By definition, the propagation speed of the surface wave profile is:

$$c = \frac{dx}{dt} = \frac{\omega}{k} = \frac{L}{T} \tag{3}$$

For a monochromatic wave, this corresponds to the phase speed (c_p), which can be readily obtained from the dispersion relationship (Eq.1).

$$c_p = \sqrt{\frac{g}{k} \tanh(kd)} \tag{4}$$

$$c_p = \sqrt{\frac{g}{k}} = \frac{g}{\omega} = \frac{g}{2\pi f} \qquad (deep\ water) \tag{5}$$

If a superposition of waves occurs, with slightly different frequency and the same direction, the phase speed of the envelop wave, that is the group velocity, can be calculated as:

$$c_{group} = c_g = \frac{\partial \omega}{\partial k} = nc \tag{6}$$

with *n* given by:

$$n = \frac{1}{2}\left(1 + \frac{2kd}{\sinh(2kd)}\right) \tag{7}$$

For deep water, $2kd/\sinh(2kd)$ approaches 0, and therefore *n*= ½. The group velocity for deep water becomes:

$$c_g = \frac{g}{4\pi f} \qquad (deep\ water) \tag{8}$$

The group velocity in deep water is thus an inverse function of wave frequency, longer, low-frequency waves travel faster, i.e., dispersive waves. For further details, the reader is referred to Holthuijsen 2007 [1].

Originating distance

With the expression for the wave speed, and knowing that waves travel on earth over great circles, the originating distance can be calculated. If wave spectral data is considered, the wave dispersion is registered by the time-series of the peak frequency. Considering two wave groups arriving to the observing location, the distance travelled by those two groups can be expressed as:

$$\begin{aligned} d_1 &= c_{g1}\Delta t_1 = c_{g1}(t_1 - t_0), \\ d_2 &= c_{g2}\Delta t_2 = c_{g2}(t_2 - t_0) \end{aligned} \tag{9}$$

Where c_g is the group velocity, *t* is the time of arrival at the observation location, and *d* is the distance travelled over the great circle. Sub-indices 1 and 2 refer to the different wave groups.

Since the base assumption is that waves are originated by the same storm at some distance *d*, and at the same time $t_0 = 0$. We have:

$$d_1 = d_2 = d; \quad and \quad t_0 = \frac{c_{g1}t_1 - c_{g2}t_2}{c_{g1} - c_{g2}} \tag{10}$$

Therefore, $d = d_1 = c_{g1}(t_1 - t_0) = c_{g1}\left[t_1 - \frac{c_{g1}t_1 - c_{g2}t_2}{c_{g1} - c_{g2}}\right]$ and after some algebraic manipulation:

$$d = \frac{c_{g1}c_{g2}}{c_{g1} - c_{g2}}(t_2 - t_1), \ with\ c_g = \frac{g}{4\pi f}$$

$$d = \frac{g}{4\pi}\frac{(t_2 - t_1)}{(f_2 - f1)} = \frac{g}{4\pi}\frac{\partial t}{\partial f} = \frac{g}{4\pi}\frac{1}{m} \tag{11}$$

where *m* is the slope of the straight line relating the peak frequency and the time of arrival. Note that if time units are seconds, the distance is obtained in meters.

Time of origin

In a similar way, the time of origin of the storm can be calculated. It can be seen from equation 10, that the time of origin is a function of the wave speed and the arrival time. Therefore, equation 10 can be expressed in terms of the peak period as:

$$t_0 = \frac{T_{p1}t_1 - T_{p2}t_2}{T_{p1} - T_{p2}} \tag{12}$$

Therefore, using the variable $T_p^* t$ (peak period times time) we find the slope $\Delta(T_p.t)/\Delta T_p$, which is associated to the time of origin.

Methodology

Spectral partitioning

The wave spectrum is the distribution of energy over a range of frequencies and all directions. In the wave spectrum, different wave systems can be identified. For instance wind-sea waves are characterized by a broad spectrum, both in frequency and direction. The frequency domain of wind-sea waves is located towards the higher frequencies, and its direction agrees well with the wind direction. Swell waves on the other hand present typically a narrower spectrum, the energy is located towards lower frequencies, and since they have been generated outside the observing area, they do not follow the wind direction. All these features can be appreciated visually in a plot of the wave spectrum (e.g., figure 1). The spectral partitioning technique [13], consists of automatically determining the different wave systems. In this technique, the spectrum is treated as an inverted catchment area [20] making an analogy with hydrological concepts. The objective is then to identify the different *basins* from that catchment area. For doing that, the algorithm group spectral points climbing to the same local peak.

Using the partitioning technique, wave systems from the grid point 1°S-93°W are identified. It is noticed in general, that wave conditions in the Equatorial Pacific Zone are characterized by four distinct wave systems: a South Westerly (SW), a North Westerly (NW), a South Easterly (SE), and a North Easterly (NE) [21]. Using these long-term characteristics, the systems can be extracted by defining frequency-direction ranges. An example of the wave spectrum and the partitioned wave systems is given in figure 1. For the present work in which the development of the methodology is the important aspect, only the South Westerly (SW) component is considered. In later works, statistics about this and the other wave systems will be covered.

Wave height clustering algorithm

The purpose of this (pre-processing) algorithm is to be able to automatically separate specific events from the time series. Figure 2 shows the time series of significant wave height (H_{m0}), panel (a), mean wave period ($T_{m-1,0}$) and peak period (T_p), panel (b), mean wave direction (θ_m) and peak direction (θ_p), panel (c). It can be seen from figure 2a, that the time series present eventual erratic variations (e.g., at days 8, 14, 22, ...). These can either be attributed to inaccuracies of the extracting procedure (frequency-direction ranges), or to the actual presence of different swell systems. In any case, there is little one can do about this behavior because it is not possible in general to set a very strict criterion to extract the SW and SE wave systems because they occur in a very close range of the frequency-direction domain.

In order to deal with the variations and to be able to distinguish separate events, the H_{m0} signal is smoothed

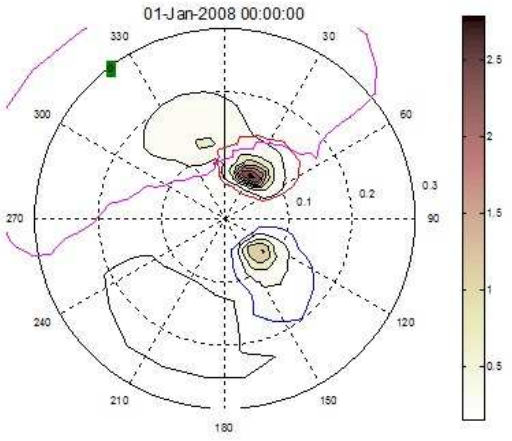

Figure 1: Example of wave systems detection results –Galapagos output point 1°S-93°W– The green dot indicates wind direction, green line indicates the wind-sea partition (not present here). Red line: South-Westerly component. Blue line: North-Westerly component. Magenta line: South-Easterly component. Black line: North-Easterly component.

using a sequence of a mean-median filter. The mean-median filter is used because it has the ability to remove single erratic deviations (like those present) while still keeping the main characteristics of the signal. The size chosen for the filter kernel is five. The resulting smooth time series are shown in figure 2a. From this signal, it is easier to identify specific events.

For the separation of each specific event, the gradient (first derivative) of the smooth H_{m0} signal is analyzed. A change of sign in the gradient (from positive to negative) indicates the presence of a valley, and therefore the limit of an event. A complementary condition is that clusters having few records (less than 3 negative points) are disregarded. This is introduced in order to overlook small local variations. The specific events identified are indicated with dashed vertical (magenta) lines in figure 2.

Analysis

The clustering algorithm works well in the H_{m0} time series, however, when looking at the wave period it is apparent that the analysis on H_{m0} is not sufficient to distinguish specific events. Particularly, events 2, 3, and 4, are composed each by two different events, although some are less important in terms of energy. It is interesting to see that in general, the mean wave period is lower than the peak wave period. This indicates a significant contribution of high frequency energy in each of the wave systems. Particularly interesting is the period between the 10^{th} and 13^{th} of January, where the mean period increases with time (wind sea behaviour), while the peak period decreases (swell behaviour). This is an indication that in that particular wave system two wave systems are merged into one. In order to visualize this, some of the spectra at those dates are provided in figure 3.

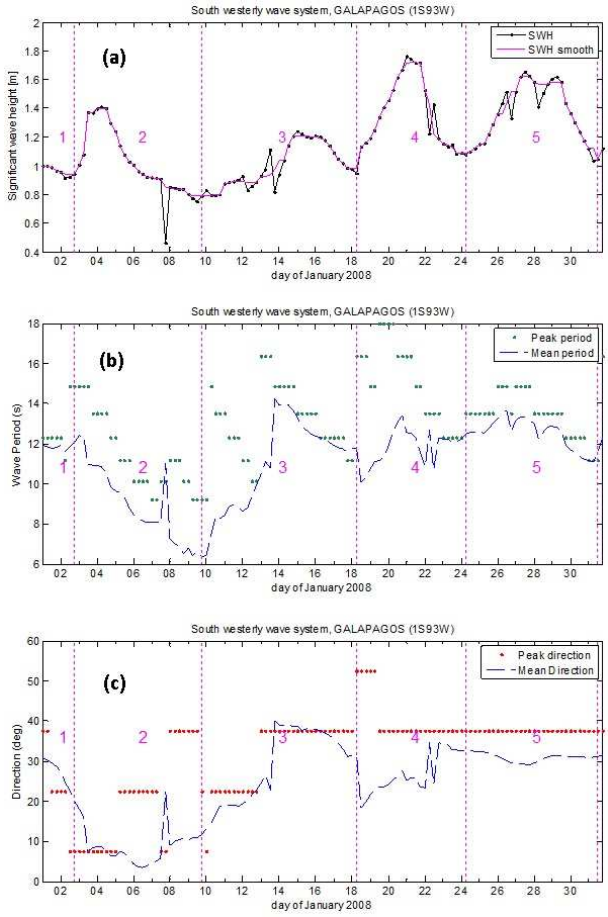

Figure 2: Time series of Significant wave height (a), mean and peak wave period (b), and mean and peak wave direction (c). Specific wave events clustered by H_{m0} are indicated.

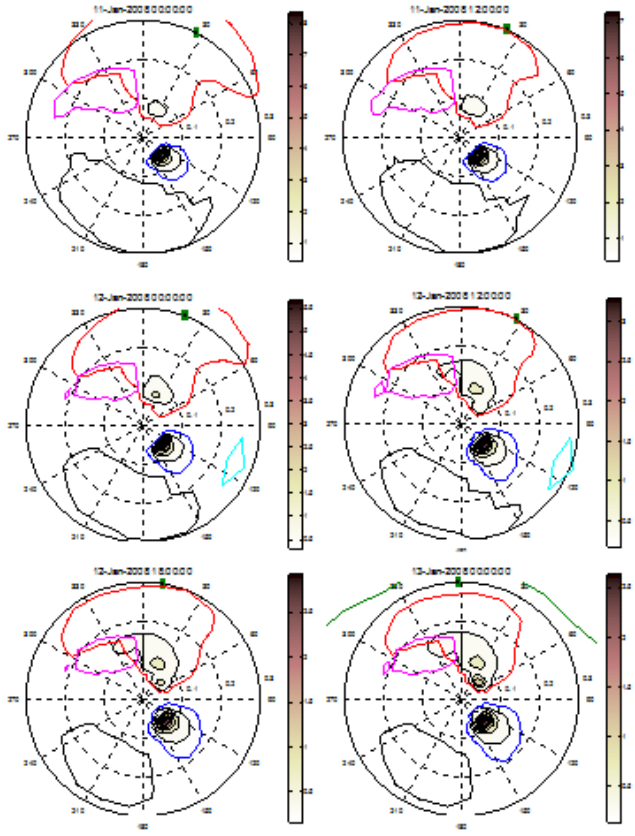

Figure 3: Wave spectra from 11-January to 13-January. South Westerly wave system marked in red.

It can be seen in figure 3 that the SW wave system (red) is actually composed of two wave systems, one with swell characteristics, narrow at low frequencies and the second one with wind-sea characteristics, wide and at high frequencies. This is related to the frequency – direction range defining the SW wave system and can be further refined. However, for the purpose of storm detection, those inaccuracies are less critical because in this particular case we are interested in the peak of the main system. This aspect however needs to be taken into account for obtaining statistics of the different wave systems or when analyzing the wind-sea component.

Wave direction provides also useful information because single wave systems may eventually change direction. For instance, in event 1 in figure 2c, direction changes from 37.5° over 22.5° to 7.5°. As mentioned before, this can be the effect of a moving storm. When constructing the algorithm, in order to determine the spatial range of the storm, both the maximum and the minimum azimuth directions are considered.

Peak frequency clustering algorithm

It is clear that from the time-series of H_{m0}, it is not possible to obtain an accurate identification of the specific wave events because consecutive wave systems with similar energy are not discernible. In order to identify those wave systems, it is necessary to analyze the time-series of the peak period. A similar smoothing procedure as for H_{m0} could be used. However, due to the discretization of the model frequency, the time-series of peak period are rather different from those of H_{m0} in the sense that peak period records repeat over time windows (figure 4a, green dots).

In order to obtain information about the gradient and its variations, records with the same frequency are grouped (figure 4a, red circles). This generates another time – series of frequency (or period), in which the frequency correspond to the frequency of the group itself and the date is found as the average date of the group. From the time-series of the grouped points (figure 4a, red circles), the gradient can readily be obtained. The change of sign in the gradient (from positive to negative) indicates the limit of a specific event.

The resulting wave events obtained from the T_p time-series are more consistent than those using H_{m0}. For instance each of the events 2 and 3 from H_{m0} (figure 4b), consist of two events according to T_p, namely 1 and 2, and 3 and 4, respectively. Therefore, the clusters obtained from the T_p time-series are used for further processing.

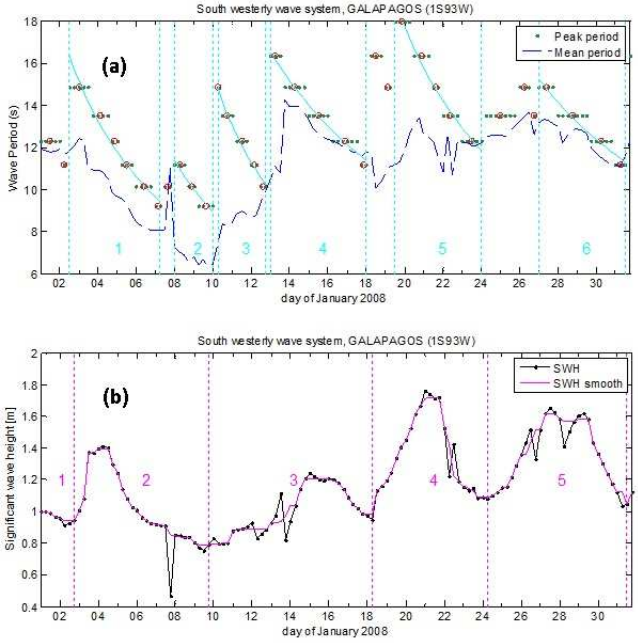

Figure 4: Time-series of peak and mean period (a), and H_{m0} (b). Specific wave events clustered by peak period (T_p) are indicated in (a) and by H_{m0} in (b), with dashed vertical lines, cyan and magenta respectively. The green dots are the actual T_p records. The red circles represent groups of records with equal T_p values. The cyan continuous lines correspond to the linear regression result for each cluster.

Linear regression

Now that the different wave events are identified, it is straightforward to compute the dispersion characteristics of the wave events. It has been seen that the peak frequency and the time of arrival are related linearly. Therefore, in order to compute the distance of origin using equation 11, we only need to compute the slope of this linear relation from the time-series of the peak frequency (figure 5). It should be noted however that although the linear trend is clear, there is some spreading in the data set, which is associated to uncertainties of the parameters of the linear regression. These uncertainties are inherent in the variable and can be attributed to either model discretization or to the displacement of the storm. If only the parameters of the straight line are computed, the output of the algorithm is a single point output (in time and space), in which the storm has to be located. However, this information is unrealistic or incomplete in the sense that storms in general have large dimensions and can be very dynamic events. Therefore, not only the parameters of the straight line are computed but also the 95% confidence intervals of the linear regression. The confidence interval provides the interval for the space and time in which the storm has developed.

Directional uncertainty

Apart from the uncertainties present in the time-series of the peak frequency, there are also uncertainties associated with direction. This can be observed for instance

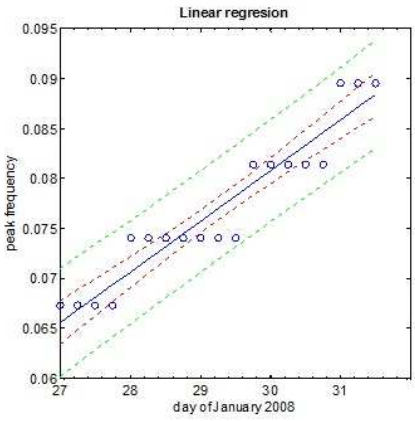

Figure 5: Linear regression fit on a peak frequency cluster. The confidence interval of slope is evaluated as it is the magnitude of interest to calculate the distance of the origin.

in figure 2c, where for a specific event, the incoming direction changes with time. In order to deal with this kind of uncertainty, the storm distance is calculated for two great circles, corresponding to the maximum and minimum azimuth directions of the specific event. With this information the location of the storm is given as a rather broad spatial domain, but given the sometimes large dimensions of the storms, results indicate that this output is consistent.

Results and Discussion

Following the procedure described above, the different events corresponding to the SW wave system at the location 1°S 93°W are analyzed for the period of January 2008. Two types of plots are provided, the first is the output of the algorithm itself, indicating the location of the storm, and the time of origin (header), and the second correspond to the atmospheric parameters, in which the location area is indicated with a red circle. The focus of this analysis is the wave event of the 29^{th} January 2008, which is a relatively high event in terms of H_{m0} (about 1.6m). The results of other events in the month of analysis are included in the appendix for reference.

The output of the algorithm indicates that waves from this event correspond to a time window relatively large that goes from the 12^{th} to the 17^{th} of January (2008). The geographical location corresponds to the south of the Australian region. When looking at the atmospheric charts, we can see that indeed the storm had a long duration, starting on the 12^{th} of January with a cyclone caused by a low-pressure front surrounded by a higher pressure environment. While evolving, this cyclone moves from west to east, and generates waves in the azimuth direction that reaches our observation location. The activity of the cyclone continues until about the 15^{th} January, decreases intensity by the 16^{th} January, and takes over again until the end of the 17^{th} January. Its effects are also visible in the time series of H_{m0}, in which the activity is relatively long ($\sim$7days) and the magnitude of H_{m0} presents some variability. It should

Wave event of the 29^{th} January 2008

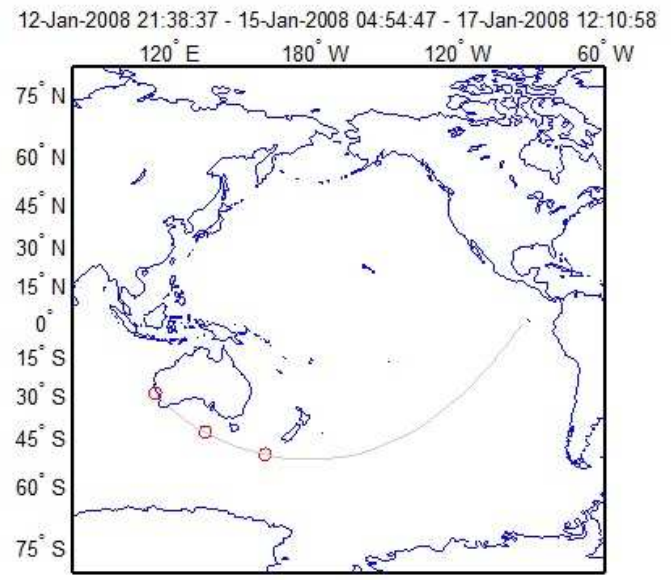

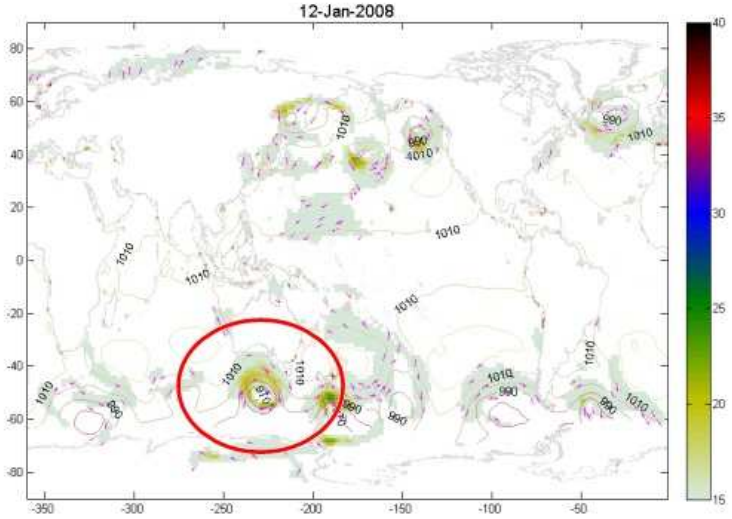

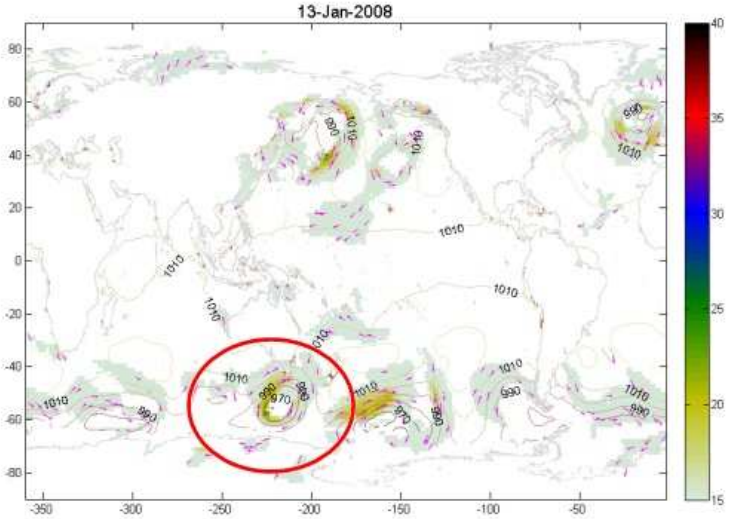

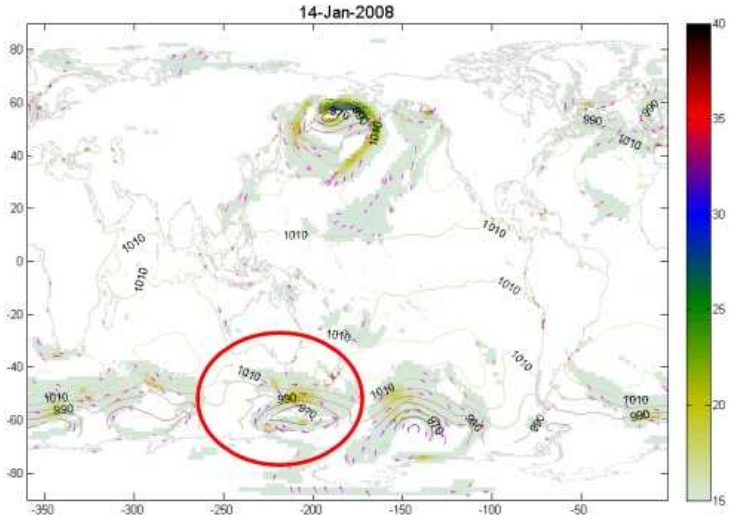
14-Jan-2008

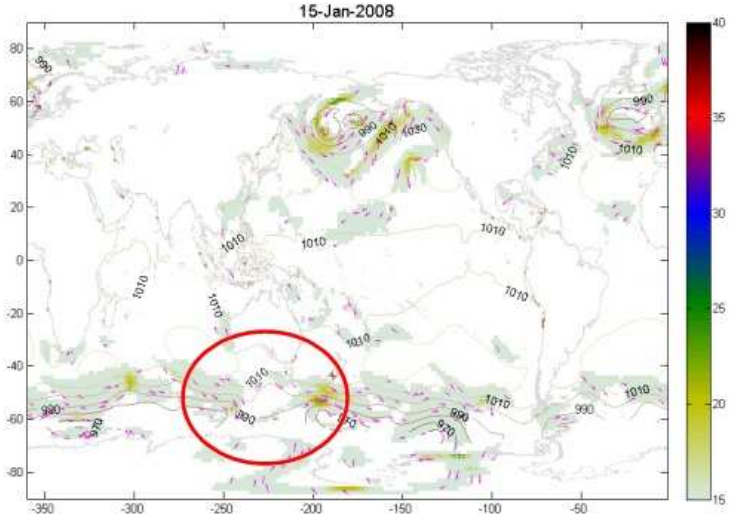
15-Jan-2008

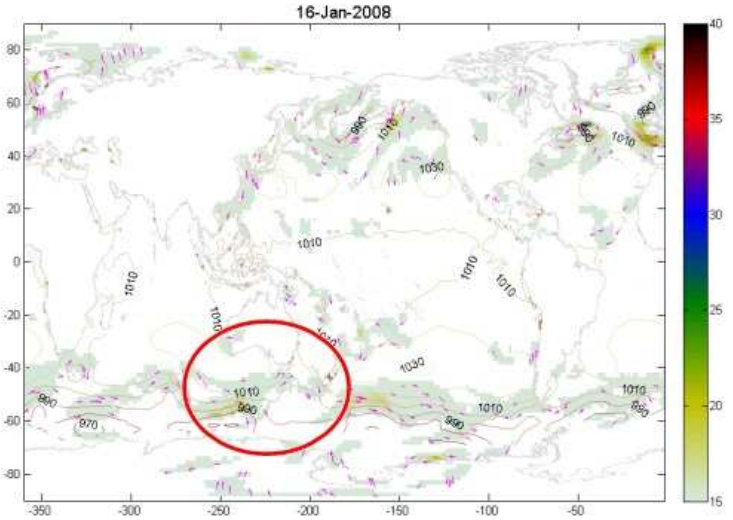
16-Jan-2008

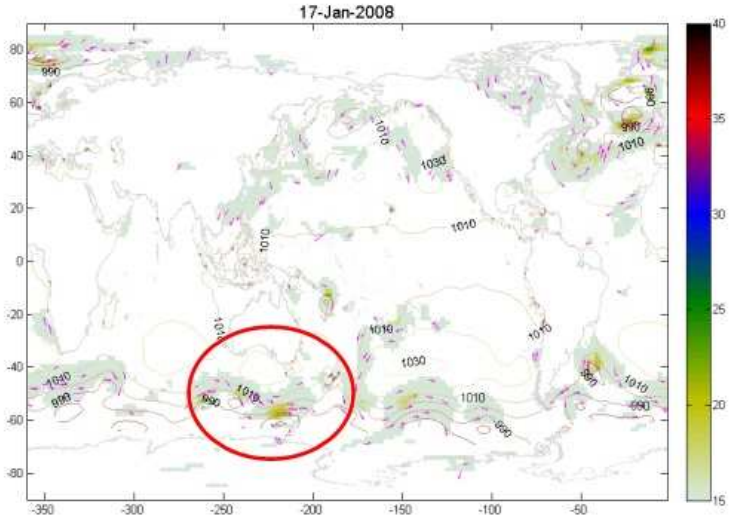

be noted also that this event does not show directional uncertainty. This is due to two main reasons. The first is that the storm itself is moving more or less well aligned with the great circle. The other is directional dispersion, enhanced by the relatively long distance.

Conclusions and Perspectives

A storm-source-locating algorithm has been developed in order to identify the zones in which waves arriving to the Equatorial Pacific Zone are generated. The output of the algorithm is consistent compared with information from the meteorological model.

The development of this algorithm is relevant since wave conditions in the Equatorial Pacific Zone are characterized mainly by swells originated in remote locations. Swell waves are more difficult to model than wind-sea waves because during the advection process they might be subject of interaction with other phenomena not represented by the model (e.g., currents, turbulence, atmosphere, Antarctic ice boundary, . . .). Therefore, a precise knowledge of this advection process is necessary.

Using the whole data set and also spectral data at other locations it is possible to perform statistics of the storm events in order to better characterize the wave conditions in the Equatorial Pacific Zone and its location of origin.

Acknowledgments

ECMWF ERA-Interim data used in this study have been kindly provided by the ECMWF. The contribution from Luigi Cavaleri (ISMAR) is much acknowledged. The collaboration of Jeison Sosa (USFQ) in complementary works has been very valuable. The author is grateful to Giuseppe Cardillo (MeriGen Research) for providing the linear regression algorithm via the MATLAB Central, File Exchange. This study has benefit from the interaction with the CD-INOCAR-LOG031-11 project. Support from the USFQ in the form of a travel grant is greatly appreciated.

References

[1] Holthuijsen, L. H. 2007. *"Waves in Oceanic and Coastal Waters"*, Cambridge University Press.

[2] Huang, C.J., Qiao, F., Song, Z., and Ezer, T. 2011. "Improving Simulations of the Upper Ocean by Inclusion of Surface Waves in the Mellor-Yamada Turbulence Scheme". *J. Geophys. Res.* 116. C01007

[3] Ardhuin, F., Chapron, B., and Collard, F. 2009. "Observation of Swell Dissipation Across Oceans". *Geophys. Res. Lett.* 36. 6-14

[4] Babanin, A.V. 2006. "On a Wave-Induced Turbulence and a Wave-Mixed Upper Ocean Layer". *Geophys. Res. Lett*. 33. L20605

[5] Munk, W.H., Miller, G.R., Snodgrass, F.E., and Barber, N.F. 1963. "Directional Recording of Swell from Distant Storms". *Phil. Trans. Roy. Soc. London A.* 255, 505–584.

[6] Snodgrass, F.E., Groves, G.W., Hasselmann, K., Miller, G.R., Munk, W.H., and Powers, W.H. 1966. "Propagation of Ocean Swell Across the Pacific". *Philosophical Transactions of the Royal Society London.* A259, 431–497.

[7] Henderson D. and Harvey. S. 2010. *"The Benjamin-Feir Instability and Propagation of Swell Across the Pacific, Mathematics and Computers in Simulation"*, Vol. In Press, Accepted Manuscript.

[8] MacAyeal, D. R., Okal, E. A., Aster R. C. 2006. "Transoceanic Wave Propagation Links Iceberg Calving Margins of Antarctica with Storms in Tropics and Northern Hemisphere". *Geophysical Research Letters*. 33, L17502.

[9] Bromirski, P.D., Sergienko, O.V., and MacAyeal, D.R. 2010. "Transoceanic Infragravity Waves Impacting Antarctic Ice Shelves". *Geophys. Res. Lett.* 37. L02502

[10] Collard, F., Ardhuin, F., and Chapron, B. 2009. “Routine Monitoring and Analysis of Ocean Swell Fields Using a Spaceborne SAR”. *J. Geophys. Res.* 114.

[11] GlobWave Project. 2012. “Demo Products, Fireworks”. *http://www.globwave.org/Products/Demo-Products/Fireworks (online)*

[12] Delpey, M.T., Ardhuin, F., Collard, F., and Chapron, B. 2010. “Space-Time Structure of Long Ocean Swell Fields”. *J. Geophys. Res.* 115.

[13] Portilla, J., Ocampo–Torres, F.J., Monbaliu, J. 2009. “Spectral Partitioning and Identification of Wind-Sea and Swell”. *J. Atmos. Oceanic Technol*. 26, 107–122.

[14] ECMWF 2010. IFS Documentation – Cy36r1, Operational implementation 26 January 2010, PART VII: ECMWF WAVE MODEL. *http://www.ecmwf.int/research/ifsdocs/CY36r1/WAVES/IFSPart7.pdf, 2011.*

[15] WAMDI group: Hasselmann, S., Hasselmann, K., Bauer, E., Janssen, P.A.E.M., Komen, G.J., Bertotti, L., Lionello, P., Guillaume, A., Cardone, V.C., Greenwood, J.A., Reistad, M., Zambresky L., Ewing J.A. 1988. “The WAM Model - a Third Generation Ocean Wave prediction Model”. J. Phys. Oceanogr.18, 1775–1810.

[16] Komen, G. J., Cavaleri, L., Donelan, M. A., Hasselmann, K., Hasselmann S. and Janssen, P. A. E. M. 1994. “Dynamics and Modelling of Ocean Waves”. Cambridge University Press, 554 pp.

[17] WISE Group: Cavaleri, L., Alves, J.H.G.M., Ardhuin, F., Babanin, A.V., Banner, M.L., Belibassakis, K., Benoit, M., Donelan, M.A., Groeneweg, J., Herbers, T.H.C., Hwang, P.A., Janssen, P.A.E.M., Janssen, T., Lavrenov, I.V., Magne, R., Monbaliu, J., Onorato, M., Polnikov, V., Resio, D.T., Rogers, W.E., Sheremet, A., Kee Smith, J., Tolman, H.L., van Vledder, G., Wolf J. and Young, I. R. 2007. “Wave Modelling: The State of the Art”. *Progress In Oceanography* 75, 603–674.

[18] Janssen, P.A.E.M. 2008. “Progress in Ocean Wave Forecasting”. *J. Comp. Phys.* 227, 3572–3594.

[19] Bidlot, J.R. 2012. “Intercomparison of Operational Wave Forecasting Systems Against Buoys: Data from ECMWF, MetO_ ce, FNMOC, MSC, NCEP, MeteoFrance, DWD, BoM, JMA, KMA, Puerto del Estado, DMI”. *Technical report*, November 2009 to January 2010, Joint WMO-IOC Technical Commission for Oceanography and Marine Meteorology.

[20] Hasselmann, S., Brüning, C., Hasselmann, K., and Heimbach, P. 1996. “An Improved Algorithm for Retrieval of Ocean Wave Spectra from Synthetic Aperture Radar Image Spectra”. *Journal of Geophysical Research*. 101, 16615–16629.

[21] Portilla, J. 2011. “Evaluación del Recurso Energético en el Mar Territorial Ecuatoriano (in Spanish), Final Report”. Technical report. CD-INOCAR-LOG031-11Guayaquil-Ecuador.

Appendix: Output results

Wave event of 04-Jan-2008: The atmospheric event that causes this wave event is pointed to the southern part of Chile. Actually this event starts around the 24-Dec-2007 and stays around until the 29-Dec-2007. It can be seen that the storm itself is moving and rotating in the domain indicated by the detection algorithm.

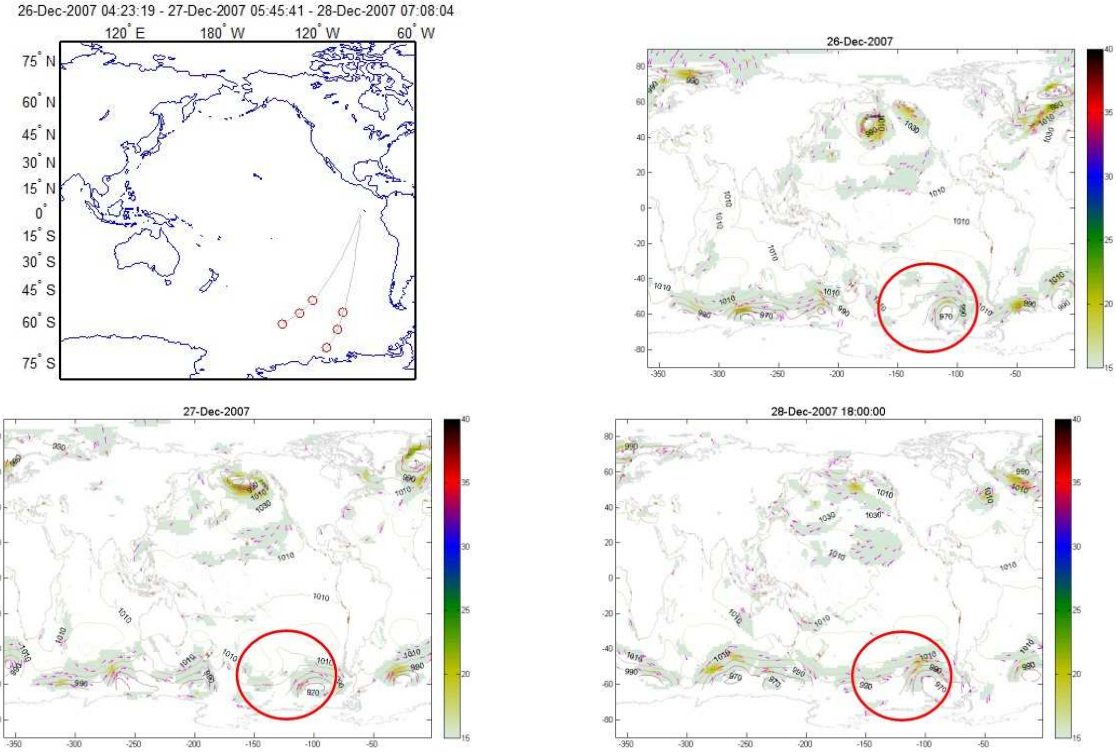

Wave event of 09-Jan-2008: The event of 09-Jan-2008 is of a relatively low magnitude (H_{m0}, 0.8m, figure 2). The ranges of directions and distances are wide, but correspond well with the domain in which the atmospheric event is taking place. In addition, the range of the originating time is consistent since this storm last some days within the calculated period.

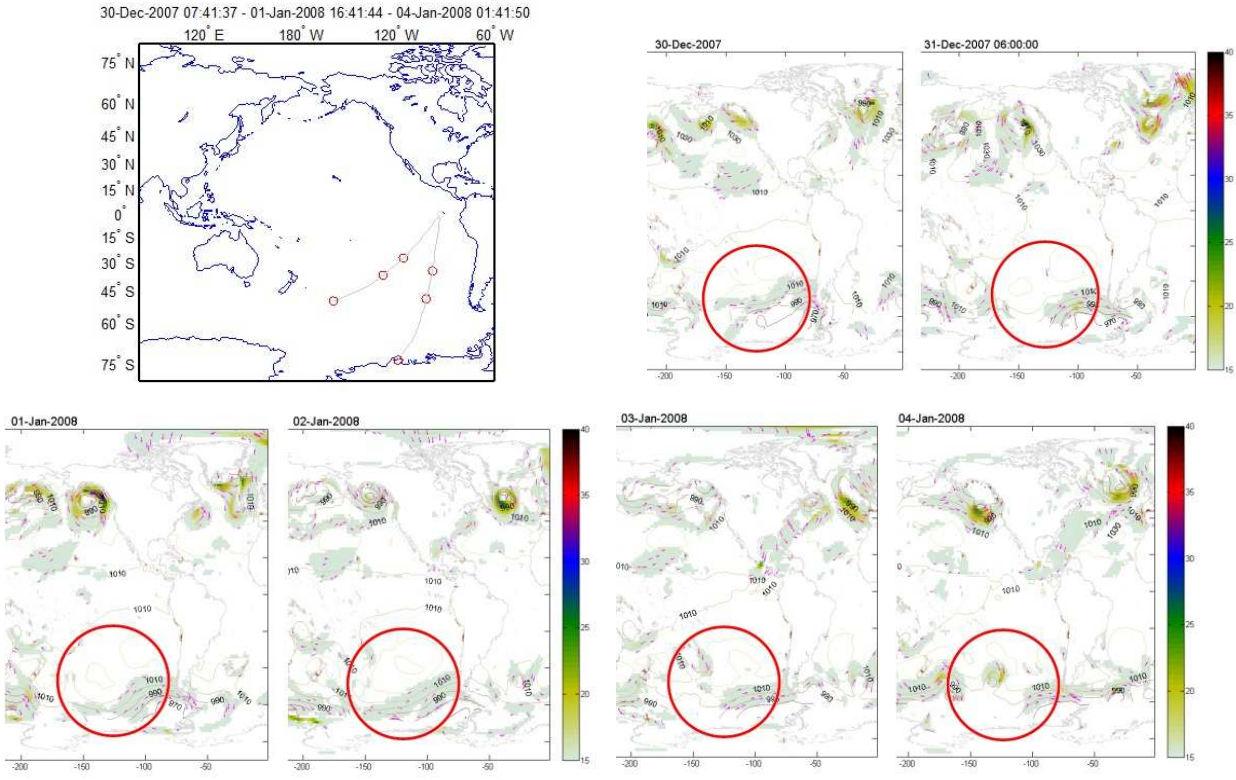

Wave event of 11-Jan-2008: This event is caused by a cyclonic storm of low magnitude in the south of Chile. The event itself in the Equatorial region is relatively low (H_s ~0.8m, figure 4). It can be seen from the figures, that in this case, the storm is relatively static at those coordinates. Therefore, at the arrival location, the direction of the waves is also constant, and the uncertainty in the distance is lower than that of the previous case.

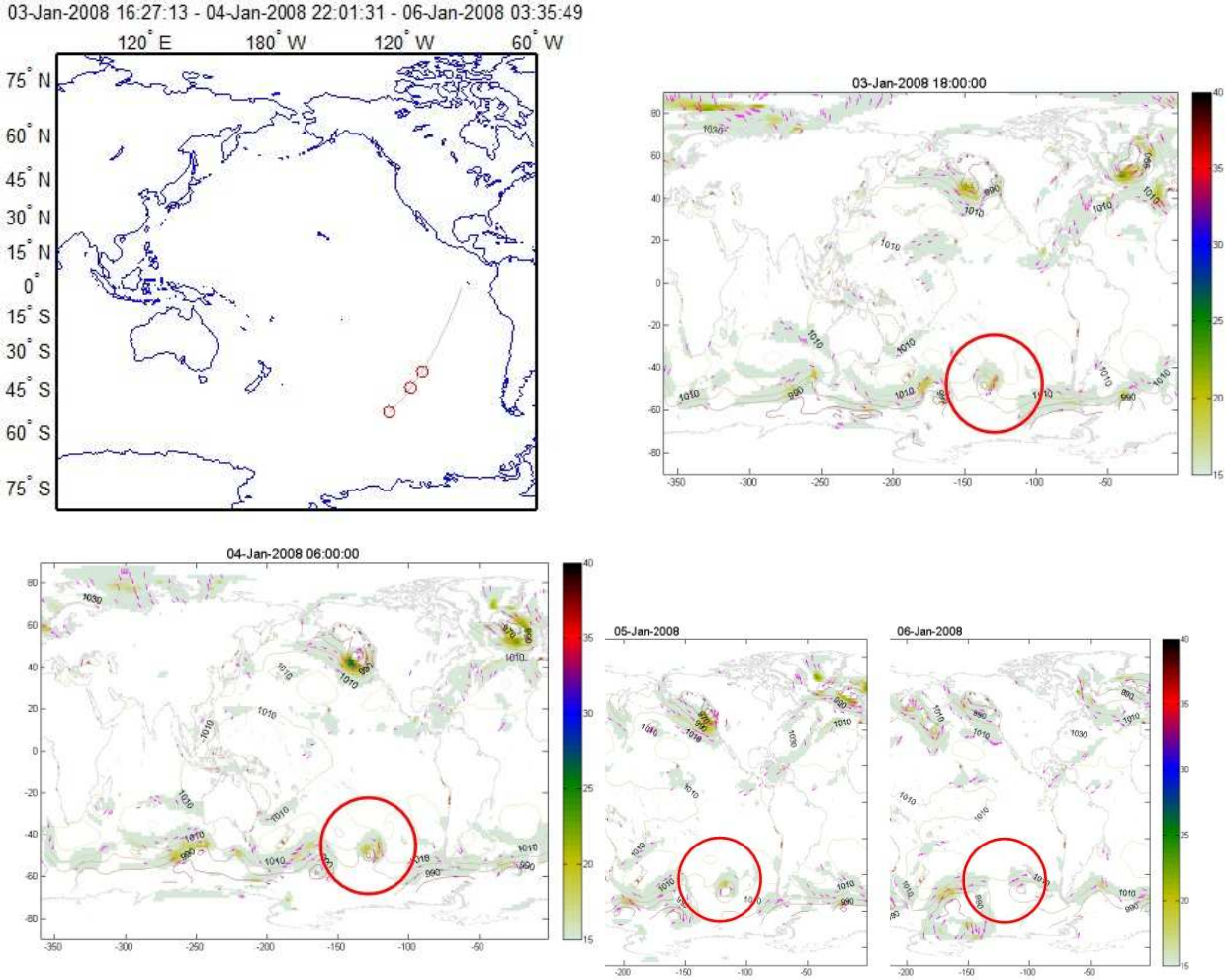

Wave event of 15-Jan-2008: This event is produced by a moderate storm in the southern part of Australia. The duration of that storm is relatively long, and extends even beyond the calculated time 4-Jan-2008, until the 8-Jan-2008. Those waves arrive also to the Equatorial Pacific (around the 9-Jan-2008) as a separate event. However this last event is not analyzed because it is composed only by 2 clusters of data points. The low uncertainty in the direction is due to two facts, one because the storm is relatively static, and second because it is produced quite far and therefore other wave directions have moved to their places due to dispersion.

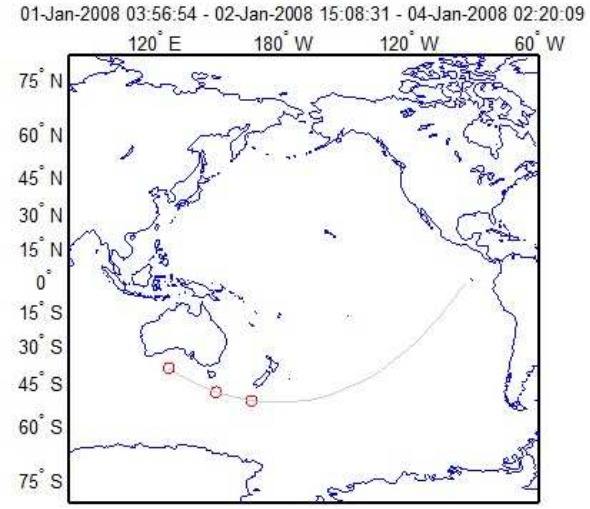

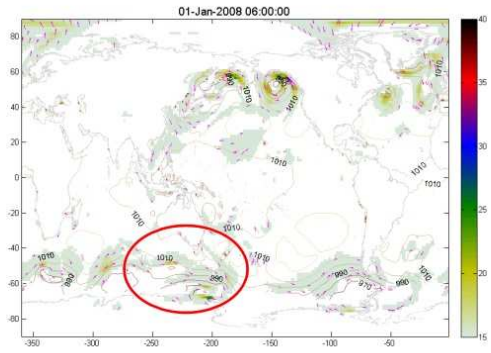

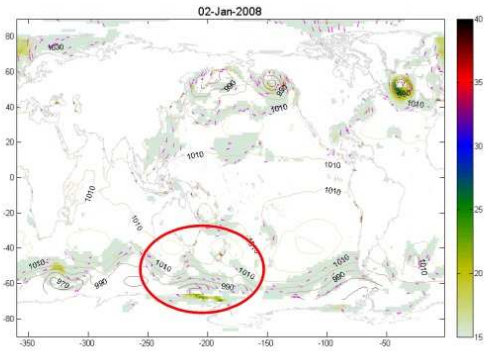

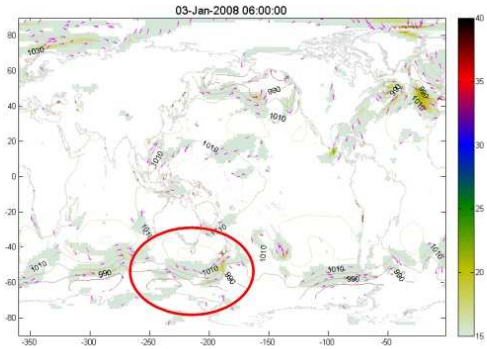

Wave event of 21-Jan-2008: This event is the largest in the time series for that month ($H_s\ sim 1.7$m, figure 4). It can be seen that actually two storm systems occur in the same period in the southeast part of Australia (and New Zeeland). The waves produced in the more westerly storm arrive few days later and show up in the time series as a different event, although some waves of those events start arriving within the 24^{th} and the 25^{th} January.